Laser-Deposited *In Situ* TiC-Reinforced Nickel Matrix Composites: 3D Microstructure and Tribological Properties

TUSHAR BORKAR,[1] JOHN SOSA,[2] JUN YEON HWANG,[3]
THOMAS W. SCHARF,[1] JAIMIE TILEY,[4] HAMISH FRASER,[2]
and RAJARSHI BANERJEE[1,5]

1.—Department of Materials Science and Engineering, University of North Texas, Denton TX 76203, USA. 2.—Department of Materials Science and Engineering, The Ohio State University, Columbus, OH 43085, USA. 3.—Institute of Advanced Composite Materials, Korea Institute of Science and Technology, Jeonbuk 565-905, Korea. 4.—Materials and Manufacturing Directorate, Air Force Research Laboratory, Dayton, OH 45433, USA. 5.—e-mail: Rajarshi.Banerjee@unt.edu

A new class of Ni-Ti-C-based metal-matrix composites has been developed using the laser-engineered net shaping[TM] process. These composites consist of an *in situ* formed and homogeneously distributed titanium carbide (TiC) phase reinforcing the nickel matrix. Additionally, by tailoring the Ti/C ratio in these composites, an additional graphitic phase can also be engineered into the microstructure. Serial-sectioning, followed by three-dimensional reconstruction of the microstructure in these composites, reveals homogeneously distributed primary and eutectic titanium carbide precipitates as well as a graphitic phase encompassing the primary carbides within the nickel matrix. The morphology and spatial distribution of these phases in three dimensions reveals that the eutectic carbides form a network linked by primary carbides or graphitic nodules at the nodes, which suggests interesting insights into the sequence of phase evolution. These three-phase Ni-TiC-C composites exhibit excellent tribological properties, in terms of an extremely low coefficient of friction while maintaining a relatively high hardness.

INTRODUCTION

Metal-matrix composites (MMCs) exhibit greater strength in shear and compression by combining the metallic properties (ductility and toughness) with ceramic characteristics (high strength and modulus).[1–4] MMCs exhibit attractive physical and mechanical properties, such as high specific modulus, fatigue strength, thermal stability, and wear resistance, that make them suitable for automotive and aerospace industries and other structural applications.[1,2] MMCs are also used in electronic applications due to their low coefficient of thermal expansion and higher thermal conductivity.[1,5–7] The properties of MMCs are mainly governed by two key factors: size and volume fraction of reinforcements as well as nature of matrix reinforcement interface.[2,8] *In situ* MMCs exhibit thermodynamic stability, good interfacial bonding, and uniform fine particle distribution in the metal matrix, which leads to better mechanical properties compared with conventional *ex situ*

MMCs.[2,9] Nickel and nickel base superalloys are widely used in aerospace applications (aircraft jet engines), land-based applications (turbines) as well as in chemical-petrochemical plants and nuclear energy sectors, due to their excellent properties such as high resistance to corrosion and fatigue and low thermal expansion.[8] Titanium carbide (TiC) has a very high hardness (2859–3200 HV), high melting point (3420 K), low density (4.93 g/cm^2), and high mechanical strength, but it is very brittle and cannot be used as a monolithic ceramic.[8,10–14] Therefore, TiC-reinforced nickel matrix composites are considered a good candidate for high-temperature refractory, abrasive, and structural applications.[8,10–14] Also, in contrast to most other metals, nickel exhibits a low wetting angle with titanium carbide, which leads to significant improvements in the interfacial bonding in case of TiC-reinforced nickel matrix composites.[15] Ni-TiC composites exhibit a good balance of properties combining the ductility and toughness of the nickel matrix with the high strength

and modulus of the TiC reinforcement, making these composites promising candidates for high-temperature structural applications.[12] Furthermore, TiC-reinforced nickel matrix composites can also be considered potential replacements for WC-Co-based wear-resistant materials[10] for surface engineering applications.[8] Ni-TiC-C composites exhibited excellent wear-resistant properties due to the presence of the graphitic phase, which plays an important role as an *in situ* solid lubricant during friction.[16] Using laser-engineered net shaping (LENS[TM]), novel monolithic composites based on Ni-Ti-C have been developed (U.S. Patent Application No. 13/769,787) that combine properties such as solid lubrication (e.g., graphite),[16] high hardness (e.g., TiC), and high fracture toughness (e.g., nickel) for structural as well as surface engineering applications. These multifunctional, monolithic composites are needed in industrial applications, such as drilling components (wear band, stabilizer, drill collar, etc.), tunnel boring, and land base turbines.

Three-dimensional (3D) microstructural characterization is very important to reveal many microstructural parameters, such as the number of features per unit volume, true size, shape, and morphology of microstructural features, and the connectivity between features, that is not revealed by simple two-dimensional (2D) microstructural characterization.[17–19] Tomographic techniques based on the 3D atom probe and transmission electron microscopy (TEM), focused ion beam (FIB) serial sectioning, synchrotron-based x-ray diffraction and tomography, and sequential mechanical polishing or micromilling are techniques particularly suited for characterizing the local structure, chemistry, or crystallography of materials in 3D, from the atomic scale all the way up to the millimeter-size volumes.[17] Serial sectioning is one of the most common and powerful methodologies used to obtain 3D microstructural data. The dual-beam FIB has become a very powerful tool for such serial sectioning and 3D microstructural reconstruction of metals with multiple phases exhibiting complex morphologies and crystallographic orientations.[17,18,20–23] Typically, in FIB serial sectioning, to characterize particular microstructural features of interest, the general rule of thumb is that there should be a minimum of 10–20 sections per feature to accurately represent its shape and size.[17] This article mainly focuses on 3D microstructural characterization of novel laser-deposited Ni-Ti-C composites. The salient features of the present study are to investigate the 3D morphology, size scale and distribution of TiC and graphitic precipitates in a nickel matrix, and the implications on the sequence of phase evolution during solidification.

EXPERIMENTAL DETAILS

Laser-Engineered Net Shaping (LENS[TM])

The titanium carbide (TiC)-reinforced nickel-based composites used for 3D microstructural characterization were deposited using the laser-engineered net shaping (LENS[TM]) process from a feedstock consisting of a blend of elemental nickel, titanium, and nickel-coated graphite powders. The processing details for these composites have been described in detail in previous papers,[8] but a short summary is included here for completion. The powders used for depositing the Ni-Ti-C composites consisted of commercially pure near spherical Ni (40–150 μm), pure Ti (40–150 μm), and Ni-coated graphite powders, which were premixed in a twin roller mixer with the nominal compositions 80Ni-10Ti-10C and 77Ni-3Ti-20C (refer to Ni-10Ti-10C and Ni-3Ti-20C for brevity). These composites were laser deposited in a cylindrical geometry of diameter 10 mm and height 10 mm. The LENS[TM] deposited *in situ* Ni-Ti-C composites were characterized by scanning electron microscopy (SEM) in FEI-Quanta Nova-SEM. X-ray diffraction analysis of deposits was performed using the (1.54 Cu Kα) line of the Rigaku Ultima III x-ray Diffractometer. Area fraction calculation of TiC and graphite reinforcements was done using ImageJ software, and an average of 50 SEM images were reported in this article. The details of FIB serial sectioning and 3D reconstruction are explained in the next section.

Dual-Beam FIB-SEM Serial Sectioning Methodology

This section will briefly describe the dual-beam FIB-based serial sectioning methodology employed to study the 3D microstructure characterization of these Ni-Ti-C composites. A dual-beam workstation (FEI Nova NanoSEM) equipped with a focused ion beam column employing a Gallium (Ga) liquid metal ion source, combined with a high-resolution field emission scanning electron microscope (FEG SEM), was used. Prior to the 3D serial sectioning, the stage was tilted to maintain the 52° angle between the FIB and the SEM column as shown in Fig. 1a, so that the sample surface of interest was oriented parallel to the ion beam during cross sectioning. A layer of platinum (Pt) was deposited on the top of the region of interest, which serves not only as protection but also helps in minimizing curtaining effects and provides a sharp cutting edge during serial sectioning.[17,22,24] Additionally, this Pt layer also acts as a fiducial marker during the 3D reconstruction process for proper alignment of the 2D SEM images. Prior to the serial-sectioning procedure, the sample is micro-machined into a cantilever beam geometry using the dual-beam FIB, as shown in Fig. 1b. This sample geometry has two main advantages: First, it minimizes the redeposition of milled material onto the surface of interest, and second, it eliminates the possibility of shielding of the detectors by the sample.[17] An automated serial sectioning procedure was employed using FEI's auto slice and view software. The use of an automated software routine ensures a consistent material removal rate during serial-sectioning and eliminates the need for human supervision and
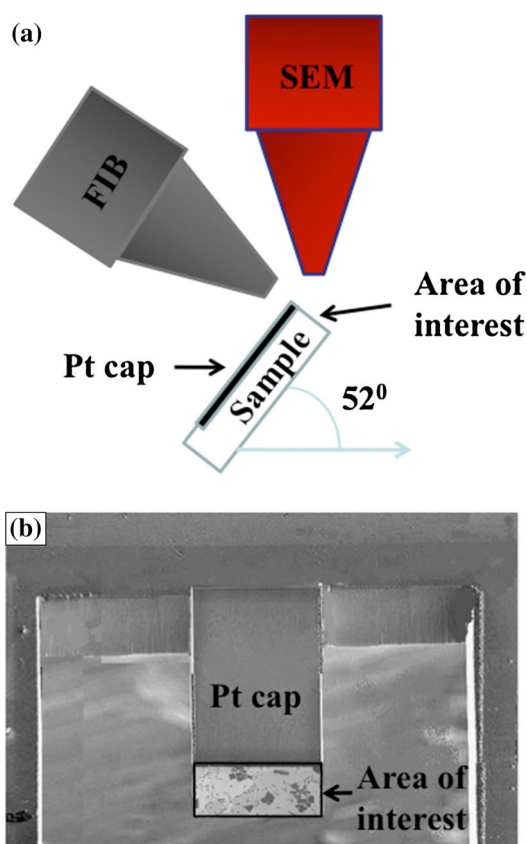
Fig. 1. (a) Schematic of the sample geometry relative to the FIB and SEM columns for serial-sectioning. (b) Representative cantilever beam sample geometry used for serial-sectioning.

interaction, so that the experiment can run for substantially longer time periods resulting in a large number of serial sections and consequently larger 3D reconstructed volumes.[17]

Three-Dimensional (3D) Reconstruction

The 2D image stack collected during the serial-sectioning procedure was reconstructed into a 3D object using the software package termed materials image processing and automated reconstruction (MIPAR[TM]) based on a MATLAB platform, developed at The Ohio State University, and the commercially available AvizoFire 6.3 software. The entire 3D reconstruction procedure consists of (I) alignment of the stack, (II) cropping of a region of interest, (III) noise filtering/thresholding, (IV) segmentation, and (V) visualization. The first four steps were performed using MIPAR[TM], and Avizo-Fire 6.3 was used for 3D visualization. In MIPAR[TM], an FFT filter was applied to minimize the curtaining effects (artifacts) obtained from FIB serial sectioning. Thresholding of TiC and graphite phases was done by applying a Gaussian blur subtraction along with the global range thresholding filter prior to segmentation of individual features. Finally, this

entire postprocessed 2D image stack was exported to AvizoFire 6.3 format for 3D visualization of TiC and graphite reinforcements.

Microhardness and Tribological Properties

The microhardness was measured using a standard Vickers microhardness tester using a 300-g load. Sliding friction and wear testing was conducted with a Falex (Implant Sciences) ISC-200 pin-on-disk (POD) system at room temperature. The samples were openly exposed in lab air ($\sim$40% RH) during the tests. Tests were performed under a 1-N normal load with a 1.6-mm-radius Si_3N_4 ball, which corresponds to an initial maximum Hertzian contact stress (P_{max}) of $\sim$1.2 GPa. The sliding speed was fixed at 50 mm/s. The ratio of tangential to normal load is the friction coefficient. At least three POD tests were run out to a total sliding distance of 140 m to achieve steady-state friction behavior.

RESULTS AND DISCUSSION

Figure 2a shows the x-ray diffraction (XRD) pattern for the as-deposited Ni-Ti-C composites of nominal compositions Ni-10Ti-10C and Ni-3Ti-20C. In the case of Ni-10Ti-10C (lower pattern in Fig. 2a), the primary diffraction peaks can be consistently indexed based on the face-centered cubic (FCC) Ni phase and the δ-TiC phase exhibiting the rocksalt (NaCl type) structure. In the case of Ni-3Ti-20C (top pattern in Fig. 2a), a peak at $2\theta \sim 26°$, corresponding to the {0002} planes of graphitic carbon, is clearly visible in addition to the FCC Ni and δ-TiC peaks. The absence of peaks corresponding to any Ni-Ti intermetallic phases is also evident in these diffraction patterns indicating that there is no reaction between nickel and titanium; rather, titanium and carbon react within a molten nickel pool to form TiC precipitates.

Backscattered SEM images from the Ni-10Ti-10C composite are shown in Fig. 2b and c, clearly exhibiting the presence of TiC precipitates with two different morphologies and size scales. The coarser and faceted carbides are likely to be the primary TiC precipitates, and the finer scale needle-like carbides are likely to be eutectic TiC precipitates, homogeneously distributed within the nickel matrix. Backscattered SEM images of the Ni-3Ti-20C composite are shown in Fig. 2d and e. These images clearly show the presence of TiC precipitates (gray) along with a substantial volume fraction of a phase exhibiting a black contrast, presumably corresponding to the graphitic phase revealed in the x-ray diffraction pattern. Ni-10Ti-10C exhibits approximately 17% (area fraction) of TiC, whereas Ni-3Ti-20C exhibits approximately 8% graphite and 4% TiC. These 2D SEM images shown in Fig. 2b–e give an idea of the overall microstructure of these composites and typically would be representative of microstructural analysis done in the past on such materials. However, the focus of the present study is
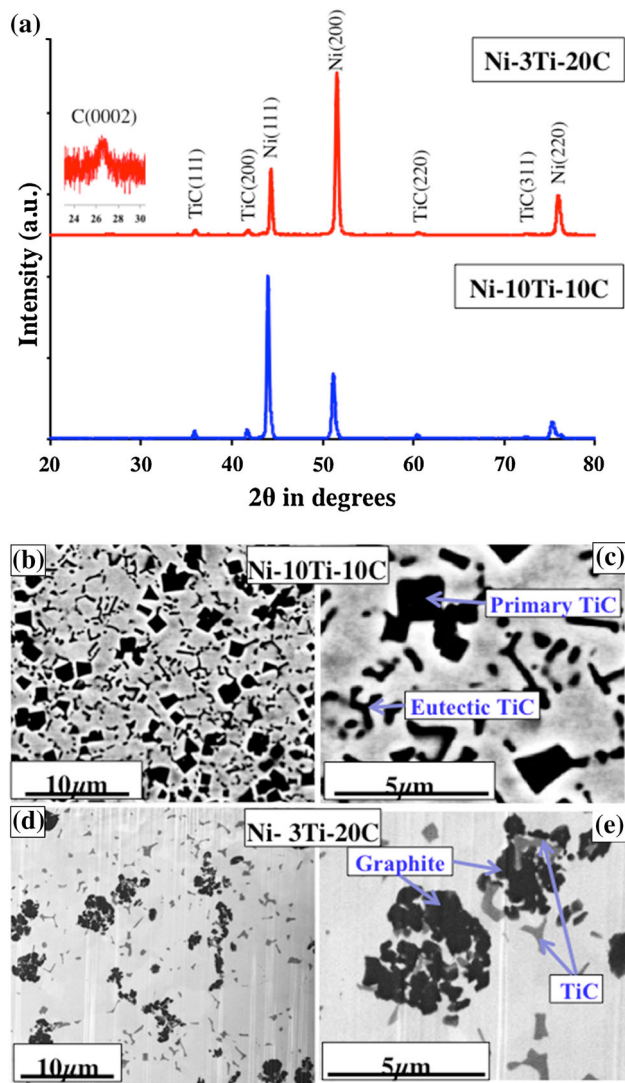
Fig. 2. (a) XRD pattern obtained from the LENS deposited Ni-Ti-C composites. (b and c) Backscatter SEM images of LENS deposited Ni-10Ti-10C composites. (d and e) Backscatter SEM images of LENS deposited Ni-3Ti-20C composites.
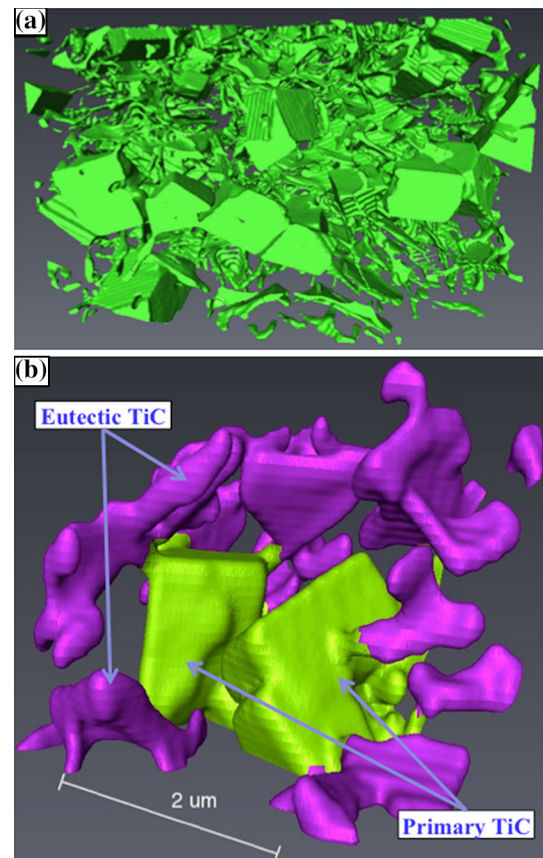

Fig. 3. (a) 3D reconstruction of Ni-10Ti-10C composites obtained from the 2D SEM image stack. (b) Cropped version of 3D reconstructed volume of Ni-10Ti-10C showing primary and eutectic TiCs.

a more detailed 3D analysis of the microstructure via serial sectioning in the dual-beam FIB and subsequent reconstruction of the 3D volume, as discussed below.

The reconstructed 3D volume corresponding to the Ni-10Ti-10C composite is shown in Fig. 3a. A cropped version of the entire 3D volume is shown in Fig. 3b for better visualization purposes. In the cropped view, the primary TiC precipitates have been colored in green, and the eutectic TiC precipitates are represented in purple. Although the appearance of this 3D microstructure is rather complex (Fig. 3a and b), it clearly highlights the following salient aspects of this microstructure:

1. The primary TiC precipitates exhibit a cuboidal morphology.
2. The eutectic TiC precipitates appear to exhibit a plate-like morphology in most cases unlike the

needle-like morphology revealed by 2D SEM observations. Some needle-like eutectic TiC precipitates are also visible in the 3D reconstruction.
3. The eutectic TiC precipitates appear to be interconnected forming a 3D network with the larger primary TiC precipitates located at the nodes of this network.

The connectivity between the carbide precipitates is impossible to discern based on the 2D SEM images in Fig. 2, without the aid of the 3D reconstruction. The eutectic TiC precipitates that are connected to the primary TiC are possibly nucleated from the primary precipitate during solidification.

Figure 4a shows the 3D reconstruction of the Ni-3Ti-20C composite. The major challenge in 3D reconstruction of these Ni-3Ti-20C composites compared with the Ni-10Ti-10C composites is the presence of two different precipitates phases, i.e., TiC and graphite. During post-processing of 2D SEM images, both phases (TiC and graphite) were thresholded differently and then exported to reconstruct the 3D volume. The TiC precipitates are yellow in color, and the graphite bundles are pink colored. The carbide precipitates (yellow) are clearly connected to each other and form a complex network
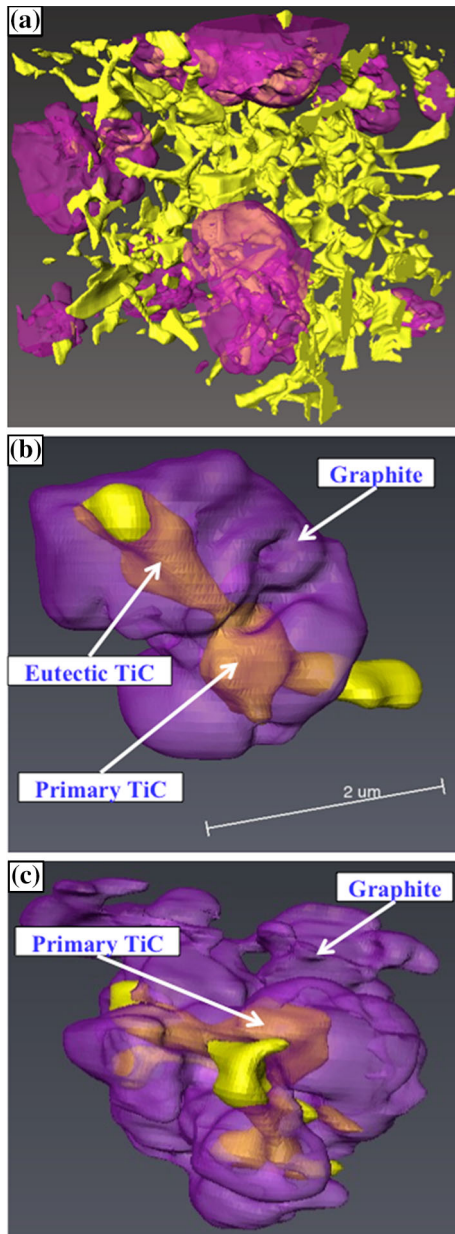
Fig. 4. (a) 3D reconstruction of Ni-3Ti-20C composite obtained from the 2D SEM image stack. (b) and (c) Cropped sections of the 3D reconstructed volume, shown in (a), of the Ni-3Ti-20C composite clearly showing primary TiC precipitates engulfed by graphite as well as the connection of the eutectic TiC precipitates to the primary TiC precipitates, forming a 3D network.

in 3D. This connectivity between the carbide precipitates is nearly impossible to visualize based on the 2D SEM images shown in Fig. 2. The distinction between the cuboidal primary TiC precipitates and the plate or needle-shaped eutectic TiC precipitates is more difficult in this case because the primary precipitates are smaller in size as clearly shown in the higher magnification views of cropped sections of the 3D reconstruction in Fig. 4b and c. Furthermore, most of the cuboidal primary TiC precipitates

are engulfed by graphite bundles (pink) as shown in both the higher magnification sections in Fig. 4b and c as well as in the overall reconstruction in Fig. 4a. Referring to the 2D SEM images shown in Fig. 2d and e, there is a gap between the TiC precipitates and the graphite bundles, and it is very difficult to comment on their interconnectivity and association based on these images. The 3D reconstructions shown in Fig. 4 conclusively reveal the true nature of the connection between the carbide precipitates and the graphitic bundles in this microstructure. Referring to the 3D reconstructions shown in Fig. 4, the eutectic TiC precipitates in the case of the Ni-3Ti-20C composite exhibit both plate-like and needle-like morphologies. The volume fractions of the different phases, in both types of composites, have also been calculated using the 3D reconstructions. The results indicate that Ni-10Ti-10C exhibits approximately 17% of TiC, whereas Ni-3Ti-20C exhibits approximately 7% graphite and 5% TiC, which is in good agreement with the values computed from the 2D area fractions. Based on these phase fractions, it is possible to recalculate the nominal compositions of the two types of composites as Ni-17Ti-17C and Ni-5Ti-12C. These corrected composition values will be employed in the subsequent section discussing the sequence of phase evolution in these composites.

Modeling the sequence of phase evolution in the Ni-17Ti-17C and Ni-5Ti-12C composites has been carried out using a simple phase diagram analysis of the Ni-Ti-C ternary phase diagram. Therefore, isothermal sections of the Ni-rich corner of the Ni-Ti-C phase diagram, at four different temperatures, computed using commercially available solution thermodynamic models (PANDAT[TM] from CompuTherm), are shown in Fig. 5 a–d. The points corresponding to the Ni-17Ti-17C (marked by a circle) and Ni-5Ti-12C (marked by a square) compositions have also been indicated on each of the isothermal ternary sections. A pseudo-binary section of the same ternary system between TiC and Ni has been plotted in Fig. 5e.[11] At a very high temperature of 2725°C, both compositions lie in the single liquid phase region. Reducing the temperature to 2500°C results in the Ni-17Ti-17C composition lying within the liquid + primary TiC two-phase field, which suggests that primary TiC precipitates will nucleate and grow in this composite. Subsequent continuous cooling of the same composition to lower temperatures increases the volume fraction of the primary TiC precipitates, and eventually at a temperature of ~1280°C, the remaining liquid in the system undergoes a pseudo-binary eutectic solidification to form eutectic Ni+ eutectic TiC as shown in Fig. 5e. Contrastingly, the Ni-5Ti-12C composition exhibits a different sequence of phase evolution, starting with a single liquid phase at high temperatures (>2500°C). Continuous cooling of this composition initially results in the primary solidification of TiC at temperatures ~1800°C (Fig. 5c), and at even
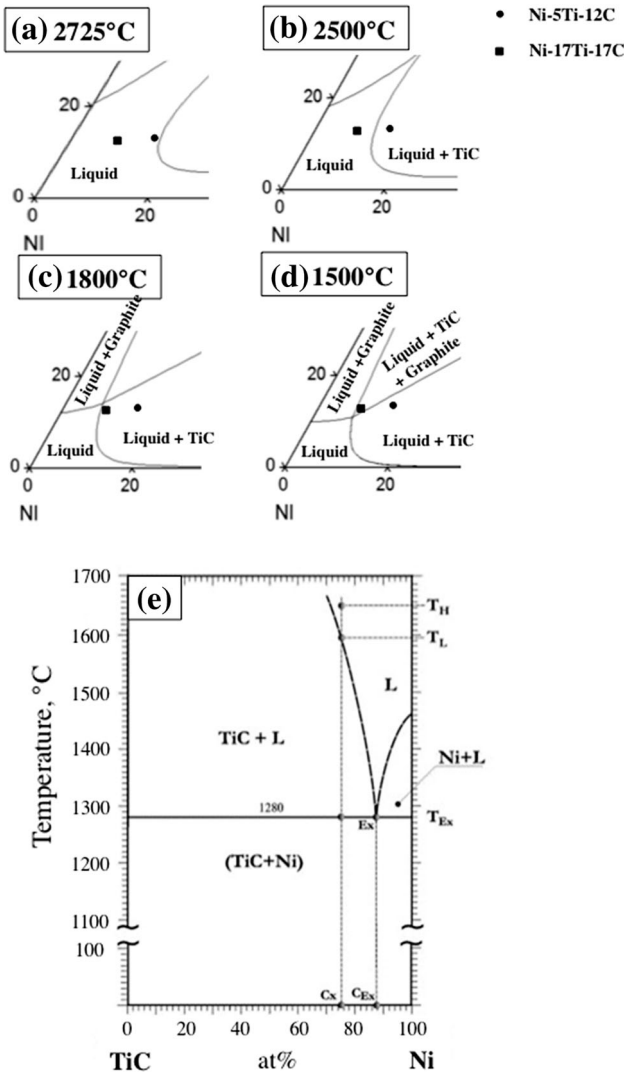
Fig. 5. Isothermal sections of Ni-rich corner of the Ni-Ti-C ternary phase diagram at (a) 2725°C, (b) 2500°C, (c) 1800°C, and (d) 1500°C temperatures. (e) A pseudo-binary section of the same ternary system between TiC and Ni.[11]

Table I. Microhardness values for the different Ni-Ti-C composites investigated in the present study in comparison with pure Ni

Composite sample	Hardness (HV)
Pure Ni	165 ± 6
Ni-3Ti-20C	240 ± 6
Ni-10Ti-10C	370 ± 10

phase to form during solidification for both types of composites. These primary carbide precipitates exhibit a cuboidal morphology, presumably dictated by surface energy criteria. Continuous cooling results in growth of these cuboidal primary TiC precipitates within the retained Ni-Ti-C liquid, depleting it of Ti and C. In the case of the Ni-17Ti-17C composition, the retained liquid eventually undergoes eutectic solidification into Ni+ eutectic TiC. The cuboidal primary TiC precipitates act as heterogeneous nucleation sites for the eutectic carbide precipitates, resulting in the formation of a network of eutectic carbide precipitates linked at their nodes by the primary carbide precipitates, as clearly revealed by the 3D reconstructions shown in Fig. 3. The regions in between this network form the pure Ni grains. In contrast, although the Ni-5Ti-12C composition also starts its solidification sequence by forming cuboidal primary TiC precipitates, the remaining liquid does not directly undergo eutectic solidification, but rather it forms a second solidification phase within the liquid, a graphitic carbon phase. This graphitic carbon phase forms directly in the liquid Ni-Ti-C and nucleates and grows preferentially at the primary TiC precipitates, eventually encompassing the entire carbide precipitate. Eventually, at even lower temperatures, the retained liquid undergoes a pseudo-binary eutectic solidification to form Ni+ eutectic TiC precipitates. The eutectic carbides also appear to heterogeneously nucleate and grow from the cuboidal primary carbide precipitates and form an interconnected three-dimensional network linked by the cuboidal primary carbides at the nodes.

The Vickers microhardness values for the three Ni-Ti-C composites and pure Ni have been listed in Table I. Comparing these microhardness values, the Ni-10Ti-10C composite exhibited a substantially higher hardness of the 370 VHN as compared with the 165 VHN for the LENS™ deposited pure Ni and the 240 VHN for the Ni-3Ti-20C composite. These microhardness values clearly show a trend of decreasing hardness as a function of increasing C/Ti ratio in the composite. The high volume fraction of titanium carbides (both primary and eutectic), in the case of the Ni-10Ti-10C composite, resulted in the higher microhardness value. Sample results of POD tribometry studies carried out on the LENS deposited Ni-10Ti-10C, Ni-3Ti-20C composites and
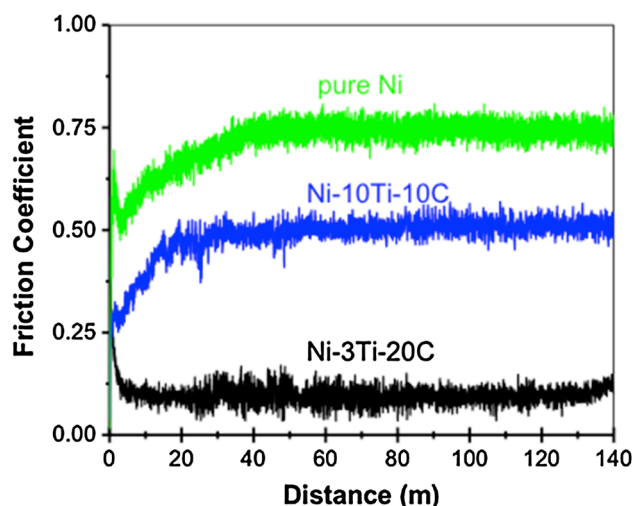
lower temperatures ~1500°C, this composition enters a liquid + TiC + C three-phase field indicating the formation of a second solidification product, C (graphite), in the liquid. Eventually at an even lower temperature ~1280°C, the remaining liquid in this case too undergoes a pseudo-binary eutectic solidification to form eutectic Ni+ eutectic TiC.

Although the sequence of phase evolution can be predicted based on the isothermal sections of the ternary Ni-Ti-C phase diagrams, the resultant microstructure is difficult to visualize without the 3D reconstructions. Thus, these reconstructions lead to a better understanding of the shape, size, distribution, and connectivity between the different phases evolving during the solidification of both types of composites (Ni-17Ti-17C and Ni-5Ti-12C). Within the liquid melt pool consisting of Ni + Ti + C, the primary TiC appears to be the first solid

Fig. 6. Steady state friction coefficient as a function of sliding distance up to 140 m for LENS™ deposited pure nickel, Ni-10Ti-10C, and Ni-3Ti-20C composites.

also pure Ni samples are shown in Fig. 6. From Fig. 6, it is clear that the presence of the TiC (and graphite) phases in these composites was beneficial in reducing the friction coefficient with respect to the pure Ni sample. Although the presence of TiC reduces the coefficient of friction, as observed in the case of the Ni-10Ti-10C composite, the presence of the lubricious graphitic phase can play a more dominant role in reducing the friction for these composites, as is clearly evident from the friction curve for the Ni-3Ti-20C composite. However, the most promising composite appears to be the Ni-3Ti-20C composite that exhibits a drastic reduction in friction coefficient ($\sim$0.1) as compared with any of the other composites,[16] mainly due to the presence of a substantial fraction of the graphitic phase as well as TiC precipitates. Thus, these Ni-Ti-C composites, especially the Ni-3Ti-20C composite, appear to be promising materials for surface engineering applications requiring high hardness with improved solid lubrication.

CONCLUSION

Novel *in situ* Ni-Ti-C composites have been deposited using the laser-engineered net shaping (LENS™) process. Although the Ni-10Ti-10C composite exhibits a large volume fraction of primary cuboidal TiC precipitates as well as eutectic carbide precipitates, the Ni-3Ti-20C composite exhibits an additional graphitic phase. The 3D microstructural characterization of these composites reveals the following salient features:

1. The Ni-10Ti-10C composite consists of a complex interconnected network of carbide precipitates with primary cuboidal TiC precipitates at the nodes of the 3D network, connecting plate-like (needle-like in some cases) eutectic TiC precipitates.

The primary carbides appear to act as the heterogeneous nucleation sites for the eutectic carbides.

2. The Ni-3Ti-20C composite also consists of an interconnected network of carbides, comprising primary carbide precipitates at nodes with eutectic carbides connecting them, but the smaller scale cuboidal primary carbide precipitates in this case are engulfed by graphitic bundles, a second primary solidification product.

Such 3D characterization leads to a better understanding of the sequence of phase evolution during solidification in these novel composites. Tribological and mechanical property measurements reveal that the steady-state friction coefficients for these Ni-Ti-C composites are significantly lower than that of pure Ni, although their microhardness is substantially higher, making them promising candidates for surface engineering applications that require both solid lubrication and high mechanical hardness. Comparing the different Ni-Ti-C composites investigated in this study, the Ni-3Ti-20C composite appears to exhibit the best balance of properties[23] with the lowest coefficient of friction as compared with pure Ni and Ni-10Ti-10C, and a microhardness that is greater than pure nickel, although being somewhat lower than the Ni-10Ti-10C composites.

ACKNOWLEDGMENTS

REFERENCES

1. S.R. Bakshi, D. Lahiri, and A. Agarwal, *Inter. Mater. Rev.* 55, 41 (2010).
2. N. Saheb, Z. Iqubal, A. Khalil, A. Hakeen, N. Aqeel, T. Laoui, A. Qutum, and R. Kirchner, *J. Nanomater.* 2012, 1 (2012).
3. S.C. Tjong and Z.Y. Ma, *Mater. Sci. Eng. R* 29, 49 (2000).
4. D.B. Miracle, *Compos. Sci. Technol.* 65, 2526 (2005).
5. S. Rawal, *JOM* 53, 14 (2001).
6. S. Cho, K. Kikuchi, T. Miyazaki, K. Takagi, A. Kawasaki, and T. Tsukada, *Scr. Mater.* 63, 375 (2010).
7. K. Zhuang and L. Wang, *Nanosci. Nanotechnol. Lett.* 4, 454 (2012).
8. S. Gopagoni, J.Y. Hwang, A.R.P. Singh, B.A. Mensah, N. Bunce, J. Tiley, T.W. Scharf, and R. Banerjee, *J. Alloy. Compd.* 509, 1255 (2011).
9. X. Wang, A. Jha, and R. Brydson, *Mater. Sci. Eng. A* 364, 339 (2004).
10. Z. Liu, J. Tian, B. Li, and L. Zhao, *Mater. Sci. Eng. A* 527, 3898 (2010).
11. D. Strzeciwilk, Z. Wokulski, and P. Tkacz, *J. Alloy. Compd.* 350, 256 (2003).
12. G. Xiao, Q. Fan, M. Gu, Z. Wang, and Z. Jin, *Mater. Sci. Eng. A* 382, 132 (2004).
13. Y. Li, P. Bai, Y. Wang, J. Hu, and Z. Guo, *Mater. Des.* 30, 1409 (2009).
14. D. Strzeciwilk, Z. Wokulski, and P. Tkacz, *Cryst. Res. Technol.* 38, 283 (2003).

15. N. Durlu, *J. Eur. Ceram. Soc.* 19, 2415 (1999).
16. S. Gopagoni, T. Scharf, R. Banerjee, and J. Tiley, U.S. Patent Application 13/769,787 (2013).
17. M.D. Uchic, M. Groeber, D. Dimiduk, and J.P. Simmons, *Scr. Mater.* 55, 23 (2006).
18. M.A. Grober, B.K. Haley, M.D. Uchic, and D.M. Dimiduk, *Mater. Charact.* 57, 259 (2006).
19. R.T. DeHoff, *J. Microsc.* 131, 259 (1983).
20. D.N. Dunn and R. Hull, *Appl. Phys. Lett.* 75, 3414 (1999).
21. B.J. Inkson, M. Mulvihill, and G. Mobus, *Scr. Mater.* 45, 753 (2001).
22. P. Burdet, J. Vannod, A. Hessler-Wyser, M. Rappaz, and M. Cantoni, *Acta Mater.* 61, 3090 (2013).
23. G. Gaiselmann, M. Neumann, L. Holzer, T. Hocker, M.R. Prestat, and V. Schmidt, *Comput. Mater. Sci.* 67, 48 (2013).
24. K. Scott, *J. Microsc.* 242, 86 (2011).